Driven Magnetic Particles on a Fluid Surface: Pattern Assisted Surface Flows

M. Belkin,[1,2] A. Snezhko,[2] I. S. Aranson,[2] and W.-K. Kwok[2]

[1]*Illinois Institute of Technology, 3101 South Dearborn Street, Chicago, Illinois 60616, USA*

[2]*Materials Science Division, Argonne National Laboratory, 9700 South Cass Avenue, Argonne, Illinois 60439, USA*

(Received 15 May 2007; published 9 October 2007)

Magnetic microparticles suspended on the liquid-air interface and subjected to an alternating magnetic field exhibit spontaneous formation of dynamic localized snake patterns. These patterns are accompanied by four large-scale hydrodynamic vortices located at the opposite ends of the snake patterns. We report detailed studies of these large-scale vortices and their relationship to the collective response of magnetic particles in the presence of an alternating magnetic field. We present a model based on the amplitude equation for surface waves coupled to the large-scale hydrodynamic mean flow equation. The model describes both the formation of the dynamic snake patterns and the induced structure of the experimentally observed hydrodynamic flows.

DOI: 10.1103/PhysRevLett.99.158301 PACS numbers: 82.70.Dd, 68.18.−g, 89.75.Kd

A resurgence of interest in pattern formation at the micro and nano scales has been driven by the prospect of a deeper understanding of the nature of the dynamic self-assembly phenomena [1]. From a practical point of view, self-assembly promises to provide a nonorthodox approach to the fabrication of a broad range of nanoscaled devices (for instance, novel memory storage elements based on self-assembled layers of magnetic particles). Experimental studies of nonequilibrium self-organization in ensembles of particles with long-range interactions have recently revealed a rich variety of patterns (rings, chains, rotating binary vortices, clusters) [2–8]. Analogues of parametrically-excited surface (Faraday) waves [9] have been recently discovered in a variety of systems subjected to periodic external excitations, from granular materials [3] to ferrofluids [5], and externally driven magnetic particles floating on the surface of a fluid [8,10]. While the physical mechanisms governing self-organization and pattern formation in these system are rather different, the similarity is deeply rooted in a universal mathematical description based on nonlinear amplitude equations for parametrically-excited surface waves. Thus, insights derived from analyzing of specific system can be often carried over to completely different situations.

In our earlier work, we observed a novel snake pattern composed of multisegmented quasi-one-dimensional localized structures. These structures were self-assembled from magnetic microparticles suspended on the surface of fluid and energized by an alternating vertical magnetic field [8,10]. We showed that these structures appear due to dynamic coupling between fluid-surface excitations and the collective response of particles to an external ac magnetic driving field. The observed patterns exhibit nontrivial magnetic structure: antiferromagnetic order between segments is accompanied by a ferromagnetic ordering of the chains of microparticles comprising each segment [8]. The pattern formation in this system is accompanied by nonlinear hydrodynamic surface flows.

In this Letter, we report in-depth experimental and theoretical studies of the hydrodynamic flows induced in the vicinity of the snake pattern. We demonstrate that these large-scale vortex flows can be fine-tuned by varying the frequency of the external driving magnetic field. We have developed a continuum phenomenological model which couples the amplitude equation for the surface waves with the equation for large-scale mean flow to describe the experimental observations. Our model successfully reproduces the phenomenon of nonlinear flow generation as well as provides new insight into the mechanism of dynamic pattern formation.

Our experimental setup is similar to that reported earlier [8,10]. A glass beaker (5 cm diameter) is filled with water and placed in the center of a magnetic coil (170 mm diameter) capable of creating vertical magnetic fields up to 120 Oe. Magnetic microparticles are suspended on the surface of the water and supported by surface tension. Positions of the particles are monitored using a fast CCD camera mounted on an optical microscope stage. In most of our experiments, we used 90 μm spherical nickel particles (magnetic saturation moment per particle at 4 kOe is 200 μemu). The setup is designed so that the magnetic force per particle associated with the field gradients (vertical and horizontal) is less than 1% of the gravitational force per particle. Thus, driving field inhomogeneity is not relevant to the phenomena reported below.

A static vertical magnetic field of sufficient magnitude generates a triangular lattice of particles due to repulsive dipole-dipole interactions between magnetically aligned particles. An alternating magnetic field, however, can produce surprising effects such as a self-organized localized snake pattern [8]. This pattern appears due to the following instability mechanism: as the magnetic moment of the particle aligns itself with the external magnetic field, the particle drags the surrounding fluid and consequently affects the surrounding particles. If the particles are close enough, their head-to-tail dipole-dipole attraction over-

comes the repulsion promoted by the external driving field, and a chain of particles is formed with magnetic moment pointing along the chain. Each chain further promotes the self-assembly process of another chain by producing local wavelike oscillations, creating a nonzero projection of the magnetic field onto the surface of the liquid. The characteristic length-scale of the resulting multisegmented snake pattern is closely related to the parameters of the excited surface waves [8]. The excitation of surface waves by oscillating magnetic particles responding to an alternating magnetic field is analogous to Faraday waves in ferrofluids and is the primary mechanism for the formation of snake patterns. The snake pattern in our experiment is accompanied by remarkably strong hydrodynamic surface vortex flows on an initially calm liquid. Figure 1 features a self-assembled snake pattern generated at 100 Oe, with a 60 Hz driving field. The strongest flows are concentrated at opposite ends of the snake pattern (see also the supporting movies [11]) where the centers of the vortices are located (dark spots in Fig. 1). The flow velocity can be as fast as a few centimeters per second and is determined by the frequency of the driving magnetic field: a 30 Hz snake generates 0.4 cm/s flow at its tail, while a 100 Hz pattern develops flows up to 2 cm/s. The vortex flows are fully determined by the snake pattern itself. To demonstrate this, we completely removed all free particles from the surface by means of a small (2 mm $\times$ 2 mm) permanent magnet, leaving only a ''bare'' snake pattern in the beaker. To visualize hydrodynamic flows, we added nonmagnetic tracer particles (70 μm copper spheres). We detected no significant changes in the flow pattern or in the strength of the vortices. To characterize vortex flows in the system, an effective vortex strength, Ω, can be defined as an asymptotic angular velocity of the vortex close to its core, $\Omega = \lim_{R\to 0} \frac{1}{2\pi R^2} \oint \vec{v} d\vec{l}$, where $\mathbf{v}$ is the horizontal velocity and R is the radius from the center of rotation. Figure 2 shows the effective vortex strength plotted as a function of the driving field frequency (amplitude of the field was fixed at 100 Oe). As it is seen from Fig. 2, the effective vortex strength exhibits almost linear growth with driving frequency f. Further increase of the excitation frequency induces an instability in which the entire snake pattern begins to move erratically in the container (see bottom panel of Fig. 2 and supporting movies [11]).

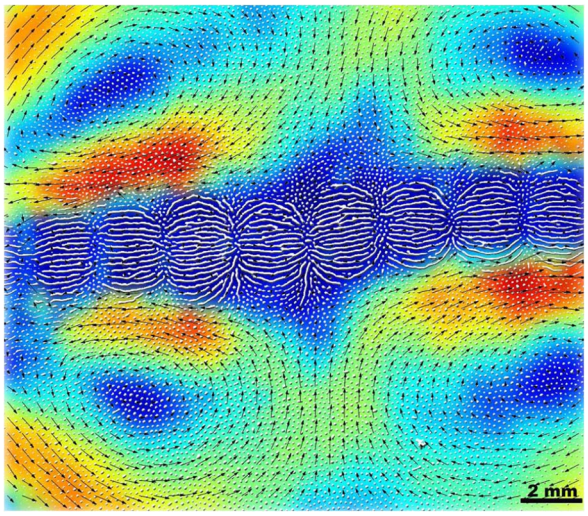

FIG. 1 (color online). Dynamic self-assembled snake structure generated by a vertical alternating magnetic field (100 Oe, 60 Hz) and induced surface flows. White round spots in the figure are 90 μm nickel particles. One sees individual particles as well as linear chains formed by particles. Arrows designate the velocity field of the surface flows obtained by means of particle image velocimetry. Background colors reflect the amplitude of the flow velocities. The flow velocity at the tails of the snake pattern reaches 1.2 cm/s.

In our earlier work [8], we described the formation of the localized snake patterns using an amplitude equation for parametric waves coupled to the conservation law for the magnetic particle density and completely neglected surface flows effects. Here, to account for the large-scale surface flow patterns observed in our system, we modify our previous model by introducing the Navier-Stokes equation for large-scale mean flow coupled to the smaller scale surface waves. A similar approach is often used in the context of large aspect ratio Rayleigh-Benard convection for the description of mean flow effects, such as rotation of spirals, spiral defect-chaos, etc. [1,12,13].

According to Ref. [8], the generation of surface waves by magnetic particles can be described phenomenologically by the following set of equations:

$$\partial_t \psi + (\mathbf{v}\nabla)\psi = -(1 - i\omega)\psi + (\varepsilon + ib)\nabla^2\psi - |\psi|^2\psi + \gamma\psi^* \phi(\rho) \quad (1)$$

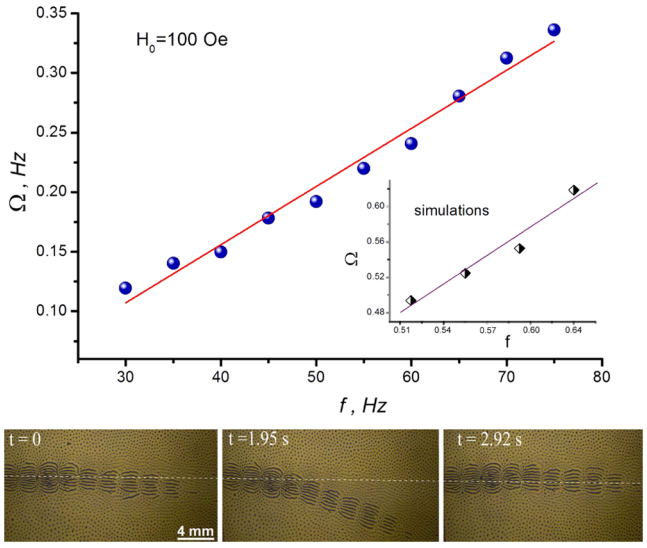

FIG. 2 (color online). Effective vortex strength Ω vs external magnetic field frequency f. Amplitude of the driving field was fixed to 100 Oe during the experiments. *Inset*: frequency behavior of the vortex strength obtained from the simulations based on the proposed phenomenological model. *Bottom panel*: onset of the snake instability (experiment: 70 Hz, 100 Oe driving).

$$\partial_t \rho + \nabla(\rho \mathbf{v}) = D\nabla^2 \rho - \beta \nabla(\rho \nabla |\psi|^2). \quad (2)$$

Equation (1) is a modified paradigm model for parametrically-excited surface waves [ψ is the complex amplitude of the surface wave $\sim \psi \exp(i\omega t) + \text{c.c.}$, $\omega = 2\pi f/f_0$] that includes parametric driving $\gamma\psi^* \phi(\rho)$ and nonlinear damping $|\psi|^2\psi$, and accounts for the presence of surface flows. The linear operator in Eq. (1) is obtained by expanding the dispersion relation near the frequency ω, and by the corresponding wave number k of the surface wave (here, $k \approx \sqrt{\omega/b}$). $\varepsilon\nabla^2\psi$ models the viscous dissipation. The original driving frequency f of the alternating magnetic field is scaled by the (arbitrary) reference frequency f_0, and time t is normalized by the reference frequency time scale $1/(2\pi f_0)$. The length is scaled by the characteristic length scale l_0 obtained from the dispersion relation for surface waves. Forcing of the waves by the magnetic field is modeled by the parametric driving term. The function $\phi(\rho)$, which accounts phenomenologically for the dependence of the forcing term on the density of particles, is chosen to be proportional to ρ for small particle densities and saturates for larger ones. Such a dependence accounts for the fact that the effect of forcing should vanish for low particle densities ($\rho \to 0$) and saturate for high densities. Equation (2) is a conservation law for the magnetic particles' density, where D is a diffusion coefficient and β denotes the amplitude of the advection term describing the concentration of particles by waves.

The evolution of the large-scale hydrodynamic velocity $\mathbf{v}$ follows from the Navier-Stokes equation

$$\partial_t \mathbf{v} + (\mathbf{v}\nabla)\mathbf{v} + \frac{\nabla p}{\rho_f} = \nu\nabla^2 \mathbf{v} + \mathbf{F}. \quad (3)$$

Here, p is the pressure, ρ_f, ν denote the fluid's density and viscosity, and $\mathbf{F}$ is a vector force due to the external driving averaged over a single period. For simplicity, we consider the situation in which the large-scale flow $\mathbf{v}$ is purely two-dimensional, allowing us to simplify Eq. (3) by introducing a stream function. We also assume that the characteristic scale of the hydrodynamic field is much larger than that associated with the surface waves.

The force term $\mathbf{F}$ requires special consideration. In the context of Rayleigh-Benard convection, which is typically described by a scalar order parameter u in the framework of the Swift-Hohenberg model equation [1], this term is proportional to $\nabla u \times \nabla\nabla^2 u$. This is because ∇u and $\nabla\nabla^2 u$ are the two simplest nontrivial vectors that can be built from the scalar order parameter. Here, we are dealing with a *complex* order parameter ψ which describes the amplitude and phase of the surface waves. Based on symmetry, one can write a general expression for the force term using the form $\mathbf{F} \sim (\psi^*\nabla\psi - \psi\nabla\psi^*)/2i$. Obviously, there is no analog of this term in the framework of the Rayleigh-Benard convection.

The onset of parametric instability can be determined by the linear stability analysis of the trivial (nonoscillating) state ($\psi = 0$, $\rho = \text{const}$). One readily derives that the parametric instability occurs at the optimal wave number $k_c = \sqrt{\frac{(\omega b - \varepsilon)}{\varepsilon^2 + b^2}}$ above some critical driving γ_c given by the

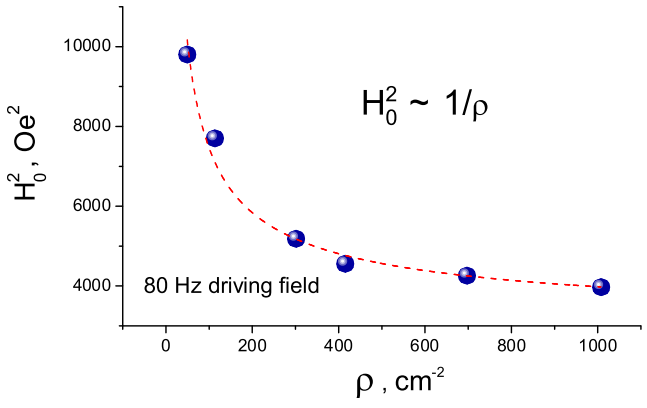

FIG. 3 (color online). Experimental critical driving field (squared) as a function of magnetic particles density. The data were taken for 80 Hz excitations. Dashed line is a fit to a $\propto 1/\rho$ dependence.

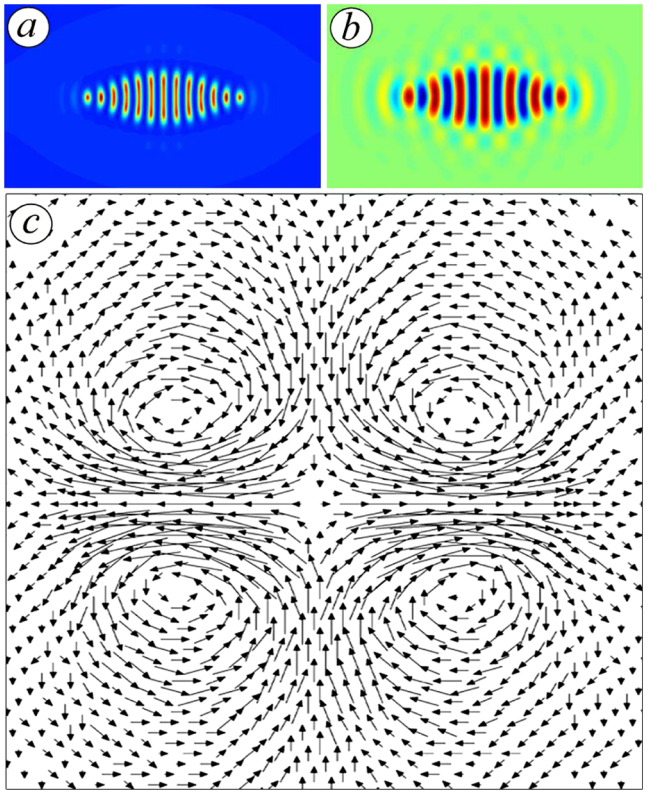

FIG. 4 (color online). Patterns and hydrodynamic flows obtained by numerical modeling: (a) density of particles at the surface of liquid. Dark color corresponds to the low density of particles; (b) Surface wave amplitude induced by the collective response of particle to the external driving. (c) velocity field generated in vicinity of the snake pattern which is located horizontally in the center of Figure. Parameters in Eqs. (1)–(3) are $\varepsilon = 1$, $b = 2$, $\gamma = 2.5$, $D = 1$, $\beta = 5$, $\omega = 3$, $\nu = 200$ in domain of 200×200 dimensionless units.

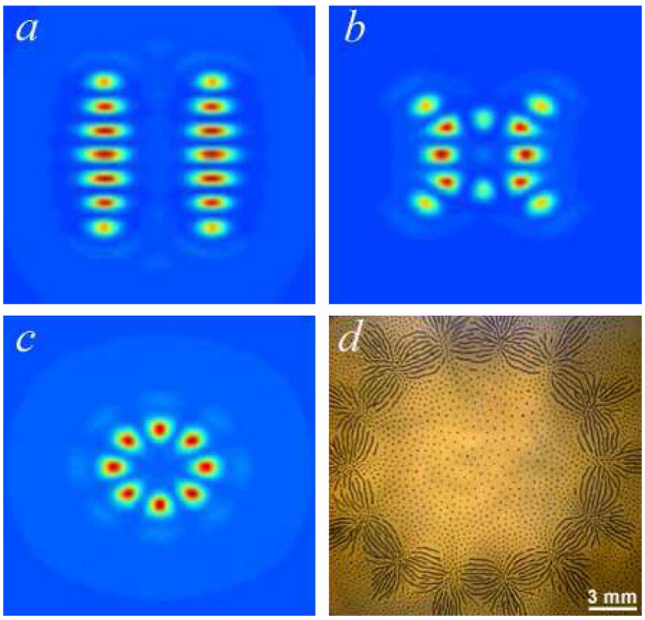

FIG. 5 (color online). Evolution of two interacting snake patterns. (a)–(c) results of simulations. Color reflects density of particles: brighter colors correspond to high densities of particles; (d) experimental realization of the round snake pattern obtained at 100 Oe, 40 Hz driving.

following expression:

$$\gamma_c \phi(\rho_0) = \frac{\omega\varepsilon + b}{\sqrt{\varepsilon^2 + b^2}}. \quad (4)$$

A finite-wavelength instability exists only if $\omega b > \varepsilon$. Equation (4) reflects an important relationship between the parameters of the driving force and the properties of the resulting snake pattern. The critical driving amplitude γ_c behaves as $\sim 1/\rho$ for small particle densities and grows linearly with the frequency of the external excitations. Since the system is insensitive to the sign reversal of the ac magnetic field, one should assume γ to be proportional to the square of the magnetic field amplitude, $\gamma \sim H_0^2$. Consequently, from the condition of parametric instability, one obtains $H_c^2 \sim 1/\rho$ law, consistent with our experimental observations (see Fig. 3).

In order to follow the evolution beyond linear instability, we solved Eqs. (1)–(3) numerically. Select patterns obtained in this way are shown in Fig. 4. Since the driving force magnitude is proportional to the local particles density, surface wave excitations occur only in particle-rich regions and rapidly decay in the depleted areas. Consequently, there is a strong correlation between the density of particles and the surface wave amplitude [see Figs. 4(a) and 4(b)]. Our model also correctly reproduces the structure of the hydrodynamic vortex flows, such as the formation of two pairs of counter-rotating vortices at the ends of the snake pattern, see Fig. 4(c). Modeling reveals that the vortex strength increases linearly with the external driving frequency, consistent with experimental observations (see inset to Fig. 2). The presence of hydrodynamic flows in the model results in more elongated snake patterns than in the previous simulations where we neglected a flow generation. In addition, simulation of two interacting snake patterns [Figs. 5(a)–5(c)] successfully reproduced a coiled-snake pattern that we have occasionally observed evolving from two nearly equal-sized snake patterns in our experiments [Fig. 5(d)].

In conclusion, we studied large-scale vortex flows in an ensemble of magnetically driven magnetic particles suspended on the surface of a liquid. Our experimental and analytical results suggest that large-scale vortices arise as a result of nonlinear coupling between surface waves induced by the magnetic particles and hydrodynamic flow in the liquid. Our phenomenological continuum model successfully reproduces the primary experimental observations, such as the formation of localized snake patterns, the structural form of the vortices, and the dependence of the vortex strength on the driving frequency. Our results yield new insights into mechanisms of self-assembly in nonequilibrium systems with competing particle-particle interactions, such as long-range magnetic and hydrodynamic forces and short-range collisions.

This research was supported by US DOE, Grant No. DE-AC02-06CH11357.

[1] M. C. Cross and P. C. Hohenberg, Rev. Mod. Phys. **65**, 851 (1993); I. S. Aranson and L. S. Tsimring, Rev. Mod. Phys. **78**, 641 (2006).
[2] B. A. Grzybowski and G. M. Whitesides, Science **296**, 718 (2002).
[3] P. Umbanhowar, F. Melo, and H. L. Swinney, Nature (London) **382**, 793 (1996).
[4] M. V. Sapozhnikov *et al.*, Phys. Rev. Lett. **90**, 114301 (2003); M. V. Sapozhnikov *et al.*, Phys. Rev. Lett. **93**, 084502 (2004).
[5] R. E. Rosensweig, Annu. Rev. Fluid Mech. **19**, 437 (1987); J.-C. Bacri *et al.*, Europhys. Lett. **27**, 437 (1994); T. Mahr and I. Rehberg, Europhys. Lett. **43**, 23 (1998).
[6] A. Snezhko, I. S. Aranson, and W.-K. Kwok, Phys. Rev. Lett. **94**, 108002 (2005).
[7] M. Belovs and A. Cebers, Phys. Rev. E **73**, 051503 (2006).
[8] A. Snezhko, I. S. Aranson, and W.-K. Kwok, Phys. Rev. Lett. **96**, 078701 (2006).
[9] M. Faraday, Phil. Trans. R. Soc. London **121**, 299 (1831).
[10] A. Snezhko, I. S. Aranson, and W.-K. Kwok, Phys. Rev. E **73**, 041306 (2006).
[11] See EPAPS Document No. E-PRLTAO-99-042741 for movies illustrating pattern assisted flows. For more information on EPAPS, see http://www.aip.org/pubservs/epaps.html.
[12] I. Aranson *et al.*, Phys. Rev. E **55**, R4877 (1997).
[13] H. S. Greenside and M. C. Cross, Phys. Rev. A **31**, 2492 (1985); M. Bestehorn *et al.*, Phys. Lett. A **174**, 48 (1993).